Section: CECN Special Issue

Proposed Associate Editor: Tomoki Fukai

Network effects of subthalamic deep brain stimulation drive a unique mixture of responses in basal ganglia output

Abbreviated title: STN DBS causes mix of output responses

Mark D. Humphries[1,2], Kevin Gurney[1]

1. Group for Neural Theory, Department d'Etudes Cognitives, Ecole Normale Superieure, 29 rue d'Ulm, 75005 Paris. France

2. Adaptive Behaviour Research Group, Department of Psychology, University of Sheffield, Western Bank, Sheffield. S10 2TN. UK

Corresponding author: M. D. Humphries

Group for Neural Theory, Department d'Etudes Cognitives, Ecole Normale Superieure, 29 rue d'Ulm, 75005 Paris. France.

E-mail: m.d.humphries@shef.ac.uk

Number of pages: ?? (Title page, abstract page, ?? manuscript pages)

Number of figures: 6

Number of tables: 0

Number of equations: 2

Number of words in whole manuscript: ??? (including abstract, references and tables)

Number of words in Abstract: ??

Number of words in Introduction: ??

Keywords: high frequency stimulation; basal ganglia; Parkinson's Disease;

Abstract

Deep brain stimulation (DBS) is a remarkably successful treatment for the motor symptoms of Parkinson's Disease. High frequency stimulation of the subthalamic nucleus (STN) within the basal ganglia is a main clinical target, but the physiological mechanisms of therapeutic STN DBS at cellular and network level are unclear. We set out to begin addressing the hypothesis that a mixture of responses in the basal ganglia output nuclei, combining regularised firing and inhibition, is a key contributor to the effectiveness of STN DBS. We used our computational model of the complete basal ganglia circuit to show how such a mixture of responses in basal ganglia output naturally arises from the network effects of STN DBS. We replicated the diversification of responses recorded in a primate STN DBS study to show that the model's predicted mixture of responses is consistent with therapeutic STN DBS. We then showed how this "mixture of response" perspective suggests new ideas for DBS mechanisms: first, that the therapeutic frequency of STN DBS is above 100 Hz because the diversification of responses exhibits a step-change above this frequency; second, that optogenetic models of direct STN stimulation during DBS have proven therapeutically ineffective because they do not replicate the mixture of basal ganglia output responses evoked by electrical DBS.

Introduction

Deep brain stimulation (DBS) has proved a remarkably successful treatment for the motor symptoms of Parkinson's Disease (Limousin et al., 1995; Deep Brain Stimulation for Parkinson's Disease Study Group, 2001). High frequency stimulation of the subthalamic nucleus (STN) within the basal ganglia has emerged as the main clinical target (Deep Brain Stimulation for Parkinson's Disease Study Group, 2001). The physiological mechanisms of therapeutic STN DBS at cellular and network level are unclear (McIntyre et al., 2004; McIntyre & Hahn, 2010).

One potential explanation is that high frequency stimulation inhibits STN neuron firing (Beurrier et al., 2001). However, while somatic inhibition of many STN neurons may occur (Beurrier et al., 2001; Tai et al., 2003; Moran et al., 2011) their axons are likely stimulated to spike (Nowak & Bullier, 1998; Miocinovic et al., 2006), others may fire somatically-generated spikes locked to the stimulation frequencies (Garcia et al., 2003, 2005) and others' firing patterns are modified (Moran et al., 2011). Correspondingly, the basal ganglia output nuclei show elevated glutamate (Windels et al., 2000) and firing rates (Hashimoto et al., 2003; Bosch et al., 2011; Moran et al., 2011) during STN high frequency stimulation. Subsequently, a theory has emerged that DBS' key therapeutic action is regularisation over-writing pathological activity (Perlmutter & Mink, 2006; Birdno et al., 2007; Birdno & Grill, 2008). Previous theoretical work has shown how high frequency stimulation of the STN could over-write the pathological activity of basal ganglia output neurons by entraining their firing (Rubin & Terman, 2004; Hahn & McIntyre, 2010), and consequently return the target structures of the basal ganglia to normal operation by removing the deleterious effect of their pathological output (Rubin & Terman, 2004; Guo et al., 2008; Dorval et al., 2010).

A common result from studies of therapeutically effective STN DBS has received comparatively little attention: that STN DBS does not just over-write, but rather causes a diversification of basal ganglia output. In the simplest manifestation, and consistent across species (human, Reese et al., 2011; primate, Hashimoto et al., 2003; rat, Shi et al., 2006), the onset of therapeutic STN DBS causes a mixture of increased and decreased firing rates in the basal ganglia output nuclei. A plausible hypothesis is that this diversification of basal ganglia output, mixing regularised firing and inhibited neurons, underlies the effectiveness of STN DBS.

We set out to begin addressing this hypothesis by extending our established computational model of the basal ganglia (Humphries et al., 2006) to incorporate a simple model of DBS effects on STN neurons. Our goals here were, first, to use the model to establish how a such mixture of responses can arise from the basal ganglia network, and whether the mixture of responses predicted by the model accurately reflected those found under therapeutic

STN DBS in parkinsonian primates (Hashimoto et al., 2003; Hahn et al., 2008). Second, we sought whether, from the "mixture of responses" perspective, the model could provide suggested resolutions to two DBS puzzles: why the clinically therapeutic frequency is above 100 Hz (Deep Brain Stimulation for Parkinson's Disease Study Group, 2001); and why optogenetic models of DBS failed to find a therapeutic effect when mimicking the direct activation of STN neurons (Gradinaru et al., 2009).

Materials and methods

We first outline our computational model of the basal ganglia. A complete description is given in (Humphries et al., 2006) – here we outline the pertinent features. Our model was explicitly of the rat basal ganglia – hence parameters such as transmission delays and neuron time constants were taken from the rat literature, and the tonic firing rates of the basal ganglia nuclei were fitted to those found in rat.

Basal ganglia circuitry

The basal ganglia are a group of inter-connected subcortical nuclei, which receive massive convergent input from most regions of cortex, and output to targets in the thalamus and brainstem. Figure 1A illustrates the macro-architecture of the basal ganglia, showing the connections between the input nuclei (striatum and STN), the output nuclei (substantia nigra pars reticulata (SNr) and globus pallidus pars internus (GPi)), and the internally-projecting globus pallidus pars externus (GPe). Figure 1B illustrates the corresponding micro-architecture of the basal ganglia, implemented in the computational models (see Gurney et al., 2001; Humphries et al., 2006, for detailed discussion). In this model the projections between the neural populations are topographically arranged to form a series of parallel loops – *channels* – running through the basal ganglia from input to output stages (Alexander & Crutcher, 1990; Hoover & Strick, 1993; Romanelli et al., 2005).

For studying DBS effects, we used our basal ganglia model with 3 channels and 72 neurons per channel in each separate structure (striatum D1, striatum D2, STN, GPe and GPi), giving 1080 neurons in total. Connection probability between nuclei was set at $p = 0.25$ for connections within a channel, and $p = 0.25/3$ for diffuse connections across channels (STN projections to GPi and GPe; local collaterals in GPe and GPi). The massively convergent input from striatum to its targets was accounted for by assigning the striatal connections a synaptic weight four times larger than all others.

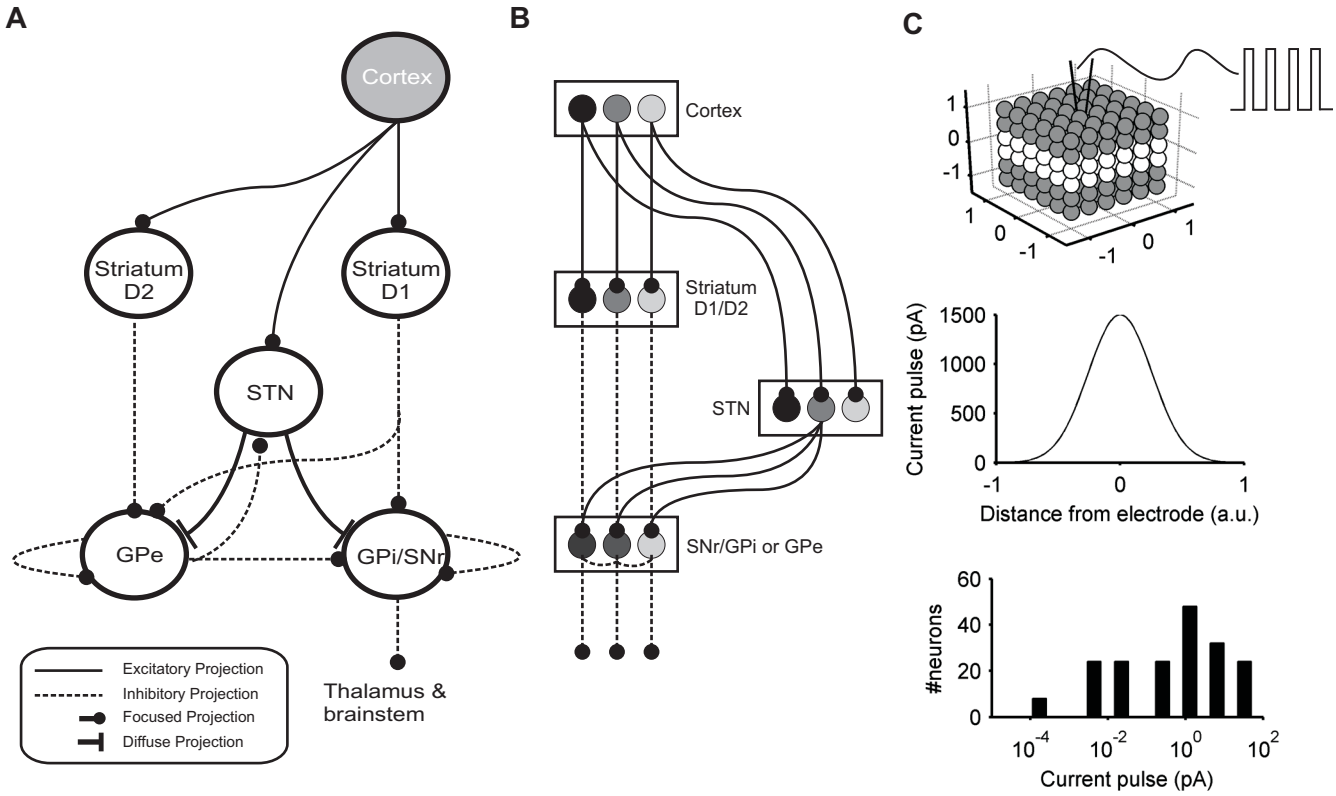

Figure 1: The basal ganglia circuitry. (A) The basal ganglia macro-circuit. Cortical input reaches both the GABAergic striatum and the glutamatergic subthalamic nucleus (STN). The striatum is divided into two populations of projection neurons, respectively expressing the D1 or D2 type dopamine receptors. The D1 population send their principal projections to the substantia nigra pars reticulata (SNr) and globus pallidus pars internus (GPi); the D2 population send their principal projections to the globus pallidus pars externa (GPe). Both SNr/GPi and GPe receive input from the STN; the GPe reciprocates that projection. Both send local projections that inhibit neighbouring neurons. Constant inhibitory output from SNr/GPi reaches widespread targets in the thalamus and brainstem. (B) The main circuit can be decomposed into two copies of an off-centre, on-surround network. Cortical inputs are topographically organised into separate groups that project to corresponding populations in the striatum and on through the SNr/GPi. In the SNr/GPi pathway, there is a balance of focussed inhibition from striatum and comparatively diffuse excitation from STN. In the D2-GPe pathway a similar overlap of projections to GPe exists, forming a second copy of this circuit. Three parallel loops are shown in both pathways; for clarity, full connectivity is only shown for the second loop. (C) Modelling deep brain stimulation as a spread-of-effect. Top: we considered our STN as a 6-per-edge cube of neurons, with each channel arranged as a $6 \times 6 \times 2$ layer of neurons, and with the DBS electrode placed at the cube's centre. Middle: the current injected into a model STN neuron with each DBS pulse was a Gaussian function of that neuron's distance from the electrode; the distance axis is in arbitrary units, with ± 1 indicating the edge of the volume. Shown for $I_{\max} = 1500$ pA. Bottom: the resulting distribution of current injected into the model STN neurons for $I_{\max} = 1500$ pA.

Model neurons

The model used current-based integrate-and-fire neurons. The change in membrane potential V of each neuron was given by

$$\tau_m \frac{dV}{dt} = -V + R\left[I_{\text{syn}} + I_{\text{ion}} + I_{\text{DBS}}\right], \tag{1}$$

with resistance R, membrane time constant τ_m, and driven by contributions from synaptic I_{syn}, ionic I_{ion}, and extrinsic I_{DBS} current sources (in the present model only STN neurons received I_{DBS}, detailed below). A neuron fired a spike when $V \geq \theta$, and was reset to the resting potential $V_r = 0$ mV; an absolute refractory period was then forced by stopping the solution of Equation 1 for 2 milliseconds. All neurons also had Gaussian noise added at every time step as a voltage deflection of V sampled from a Gaussian distribution of 0 ± 0.3 mV; this modelled both the numerous sources of noise (such as synaptic transmission failure) and the effect of unmodelled inputs to each neuron.

Synaptic input was modelled using GABAa synapses for all inhibitory connections and AMPA and NMDA synapses for all connections made by STN neurons and cortical inputs. Each synaptic event was modelled as a step-and-exponential-decay current. The current step was determined so that the average resulting post-synaptic potential peaked at $\pm$ 3 mV per input spike for GABAa and AMPA synapses, and 0.1 mV per input spike for NMDA synapses. Decay constants were set to standard values: AMPA: 2 ms; GABAa: 3 ms; NMDA: 100 ms.

Though the model was based on point-neurons, we simulated a compartmental effect of GABAa synapses as dendritic location of GABAergic synapses plays a major role in synaptic integration, and are differentially distributed on target dendrites in the basal ganglia depending on the type of projection. For each inhibitory projection type (e.g. GPe-STN), the GABAa synapses on each target neuron were stochastically assigned to either a somatic, proximal, or distal pseudo-compartment, according to the synaptic distributions taken from data (Humphries et al., 2006). GABAergic input to the proximal pseudo-compartment shunted synaptic input to the distal compartment; similarly, GABAergic input to the somatic pseudo-compartment shunted synaptic input to both distal and proximal compartments; shunting was simulated as a division of the incoming synaptic current in proportion to the number and strength of GABAa synapses in that pseudo-compartment. We had previously found (Humphries & Gurney, 2001) that this form of modelling GABAa shunting was essential for replicating the dual modes of slow bursting in the STN-GPe loop recorded in vitro (Plenz & Kitai, 1999).

The ionic contributions took two forms. First, all neurons received a tonic injection current: a positive current in STN, GPi, and GPe neurons phenomenologically modelled the current cycle underlying their tonic, pacemaker

firing (Surmeier et al., 2005) – in (Humphries et al., 2006) the positive currents were tuned to fit the tonic firing rates of these structures in awake rat; a negative current in striatal neurons phenomenologically modelled the strongly hyperpolarising effect of their inward-rectifying potassium channel (Nisenbaum & Wilson, 1995). Second, STN neurons received an additional current source modelling the calcium-channel dependent rebound bursting of these neurons (Beurrier et al., 1999; Bevan et al., 2002); the parameters were set mean values that allowed the model to replicate the duration and frequency of STN bursting in vitro (Beurrier et al., 1999; Plenz & Kitai, 1999; Humphries & Gurney, 2001).

Mean values for τ_m and R were taken from published values for each neuron type (see Humphries et al., 2006). In each instantiation of the model, values of τ_m and R for all neurons, and the burst-firing parameters for each STN neuron, were sampled from a Gaussian with a standard deviation that was 10% of the mean value.

The parkinsonian model

Our basal ganglia model is able to simulate the effects of tonic dopamine on striatal projection neurons (separately for D1 and D2-receptor expressing neurons), STN, and GPe, as detailed in (Humphries et al., 2006). Here we examined DBS effects only under parkinsonian-like conditions, and so dopamine was absent from the model throughout. In terms of our model parameters from (Humphries et al., 2006), we set $\lambda_1 = \lambda_2 = 0$. In (Humphries et al., 2006) we showed how changing the model from its normal tonic dopamine state to this parkinsonian state captured a broad range of known effects of dopamine loss on basal ganglia dynamics. First, that loss of dopamine increased the transmission of cortical oscillatory activity through the STN and GPe loop, thus increasing the correlation of neuron firing in these structures, as observed in MPTP primates and Parkinson's disease patients (for review see Hammond et al., 2007). Second, that a combined dopamine and cortical lesion uncovered the residual slow bursting in the STN-GPe loop, as observed in 6-OHDA lesioned rats (Magill et al., 2001). Third, that loss of dopamine increased the proportion of SNr/GPi neurons that increase their firing rate during putative motor commands, as observed in MPTP primates (Leblois et al., 2006b). Consequently, our simulations of STN DBS reported here were performed in a model consistent with a parkinsonian basal ganglia.

Modelling deep brain stimulation

We used a simple model of the effect of a DBS pulse on individual STN neurons, which attempted to qualitatively account for the spatial extent of tissue activated by DBS. Our starting assumption was that the change in extra-

cellular voltage evoked by a DBS current pulse decays as a function of distance from the electrode (Rattay, 1999; Miocinovic et al., 2006; Zhang & Grill, 2010), and thus induced current flow into the neuron also decays as function of distance. Here we qualitatively model this by distributing the magnitude of DBS-evoked current injection as a Gaussian function of distance d from the electrode:

$$I_{\mathrm{DBS}} = I_{\max} \exp\left[-(d/\sigma_d)^2\right]. \tag{2}$$

We considered the model STN as cube of six, equally-spaced neurons per edge of unit length, with each channel a $6 \times 6 \times 2$ layer, and the DBS source as a point electrode placed in the centre (Figure 1C). As not all STN is activated by DBS pulses (Miocinovic et al., 2006), we set the Gaussian width at $\sigma_d = 0.1812$ to give a broad range of currents I_{DBS} across the model STN (an example distribution is plotted in Figure 1C). As reported in the Results, we sought appropriate magnitudes for maximum DBS-induced current flow $I_{\max}$ by fitting to DBS response data from MPTP primates (Hashimoto et al., 2003). Unless otherwise stated, trains of DBS current pulses I_{DBS} were delivered at 130 Hz, with a width of 100 μs.

This simple model omits many proposed effects of DBS, including suppression of synaptic input, somatic inhibition of STN neurons, and direct activation of STN axons (McIntyre et al., 2004). We noted however that the resulting mixture of firing rates in STN (see, for example, Figure 2A) was consistent with the mixture of effects reported or predicted for STN high frequency stimulation: some STN neurons showed stimulus-locked firing, replicating the DBS-locked somatic or axonal generation of STN spikes (Garcia et al., 2003, 2005; Miocinovic et al., 2006); some STN neurons were partially inhibited (Tai et al., 2003; Moran et al., 2011); some completely inhibited (Miocinovic et al., 2006; Moran et al., 2011); and others showed synaptically-modulated firing patterns (Moran et al., 2011). In our model, this mixture arises entirely from the interaction between the DBS pulses into STN neurons and the effects of the STN-GPe loop in the network; but undoubtedly the actions of DBS include suppression of synaptic input and direct activation of axons (Ranck, 1975; Rattay, 1999; McIntyre et al., 2004; Miocinovic et al., 2006).

We also used a simple model of optogenetic-DBS, in which each STN neuron received the same size current pulse I_{DBS} to simulate the driving of the STN neurons by light-activated opening of channel-rhodopsin channels. Values for I_{DBS} were found by fitting to STN firing rate changes under optogenetic-DBS (Gradinaru et al., 2009), reported in the Results.

Simulations and statistics

All simulations using STN DBS were run for a total of 30 seconds, divided into 3 epochs: pre-DBS (10 seconds); on-DBS (10 seconds); post-DBS (10 seconds). Rate histograms for single neurons were computed using 1 s bins. Changes in firing rate caused by STN stimulation were detected by computing a two-tailed Mann-Whitney U-test between the pre-DBS and on-DBS epochs; we took $p < 0.05$ as indicating a significant changes in rate due to STN stimulation. Fidelity of firing to stimulation frequency was computed as the proportion of DBS pulses after which the neuron fired at least one spike before the next DBS pulse. Regularity of firing for each neuron was measured by its inter-spike interval (ISI) coefficient of variation (CV): ISI CV = s.d.(ISI) / mean(ISI).

For a detailed comparison with the data from the primate STN high frequency stimulation study of Hashimoto et al. (2003), we used a "models-as-animals" protocol (Humphries et al., 2006; Humphries & Gurney, 2007b). Briefly, a typical electrophysiological study collects a total of T neurons across N animals and approximately C cells per animal: we match this with T neurons from across N models and C neurons sampled per model; each model has a different realisation of the stochastic connectivity, and newly sampled distributions for R, τ_m, and the free parameters for I_{ion} – thus each represents a different animal. This approach circumvents issues of the differing statistical power and the differing sampling of response classes with different total numbers of neurons T, and of the differing convergence of summary statistics depending on the combination of N and C (Humphries & Gurney, 2007b). In this way, we aim to generate results whose statistical properties are comparable with their experimental counterparts, thereby enabling statistically valid claims about the "fit" between the model and the data.

Following our previous work (Humphries et al., 2006), cortical input was generated as 72 spike-trains per channel, connected to each STN and striatum neuron in that channel with a probability of 0.25. Input from cortex was modelled under a variety of recording conditions. For replications of the data from awake, resting, head-fixed primate (Hashimoto et al., 2003), we generated Poisson trains of 3 Hz (this input was used for all simulations unless otherwise specified). For optogenetic-like simulations in awake, freely-moving rats (Gradinaru et al., 2009), we generated Poisson trains of 15 Hz. For tuning of the optogenetic-DBS model to changes in STN firing rate, recorded in rat under isoflurane anaesthesia (Gradinaru et al., 2009), we simulated the cortical slow-wave at ~ 1 Hz induced by this anaesthetic (Ferron et al., 2009), following our similar simulations of urethane anaesthesia (Humphries et al., 2006): every cortical train synchronously alternated between active up- and silent down-states every 0.5 seconds; during each up-state, each train was assigned uniformly-spaced spikes at a rate f sampled from Gaussian 24 ± 1.15 Hz, and each spike was then jittered by δ_t seconds, sampled from a Gaussian of $0 \pm 0.25/f$.

Results

STN high-frequency stimulation drives mixture of responses in basal ganglia output

We begin by qualitatively illustrating the model's two main predictions for the network effects of STN high frequency stimulation. First, that regular, high-frequency, pulsed, positive current stimulation of the STN drives a mixture of changes in the basal ganglia output nuclei. Second, that this mixture of responses is a network effect, arising from variations in the balance of glutamatergic input (from STN) and GABAergic input to each neuron in the basal ganglia output nuclei.

Figure 2A shows the spike output of all model neurons in the STN, GPe, and GPi immediately preceding and following the onset of 130 Hz stimulation of the STN. Onset of stimulation entrained some STN neurons, while others were silenced, and others continued to fire irregularly (Figure 2C). All these effects were due entirely to the network response to the stimulation, as we did not explicitly model synaptic suppression, somatic inhibition, or any other source of inhibition to the STN other than synaptic input (which is not to say that those factors do not contribute to the effect of STN DBS). In GPe and GPi a subset of neurons also became entrained to their STN input, and increased their firing rate and regularity; but others showed reduced activity, and others did not change their firing rates. Figure 2B shows examples from GPi of each firing rate response to STN stimulation.

Figure 2C shows that a subset of GPi neurons became tightly locked to the stimulation frequency and hence highly regularised in their output. Across the whole GPi, STN stimulation caused significant excitation and significant inhibition of responses in approximately equal proportions, with a small proportion of unresponsive neurons (Figure 2D).

While the excitatory responses were directly driven by STN firing, the equally prevalent inhibitory responses were a little counter-intuitive. By construction, we know the model contains only three sources of GABAergic input to GPi neurons: the striatum, the GPe, and local collaterals in GPi. The striatum was barely active under the background cortical firing input, and unaffected by STN stimulation. Lesioning the GPe to GPi pathway in the model reduced the proportion of inhibitory responses in GPi (Figure 2D). An additional lesion of the GPi local collaterals further decreased the proportion of inhibitory responses in GPi (Figure 2D). With all GABAergic sources accounted for, there remained only a small proportion of inhibitory responses in GPi following STN high frequency stimulation; thus, under this model of DBS, the silencing of some STN neurons makes a small contribution to the significant reduction of output neurons' firing rates. The model thus shows that a mix of responses in basal ganglia output naturally arises from the network effects of STN high frequency stimulation.

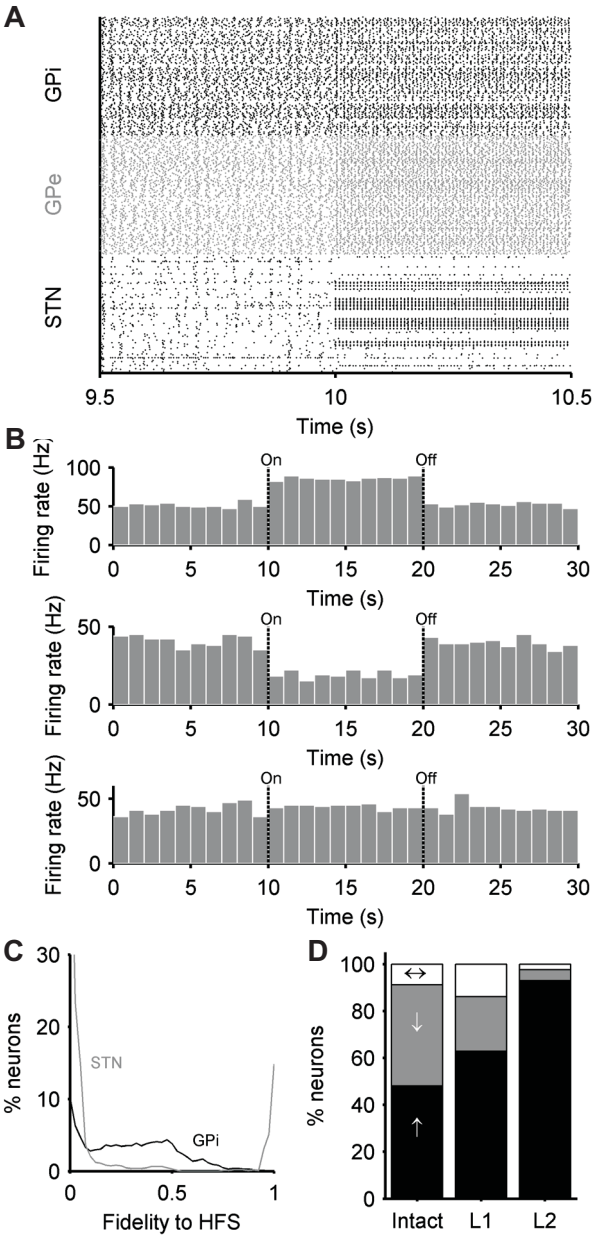

Figure 2: Subthalamic high-frequency stimulation evokes a mixture of responses in the output of the model basal ganglia. (A) Raster plot showing a one second snapshot of the outputs of all model STN, GPe, and GPi neurons in an example simulation. Deep brain stimulation (130 Hz, 100 μs width, $I_{\max} = 1500$pA) was switched on at 10 s. Some STN neurons became entrained to the stimulation, others were immediately silenced. (B) Example GPi neurons showing the mixture of firing rate responses to STN high frequency stimulation: excitation (top), inhibition (middle), and no change (bottom). These three neurons are from the simulation in panel A. (C) Distribution of STN and GPi neuron fidelity to the 130 Hz stimulation of STN: a fidelity of 1 indicates that the neuron fired after each DBS pulse; a fidelity of 0 indicates complete inhibition during the on-DBS epoch. (D) Distribution of firing rate responses to STN high frequency stimulation over all neurons in GPi: significant excitation (black), significant inhibition (grey), and no response (white). The three bars correspond to: the intact model (from panel A); L1: the same model with a lesion of the GPe to GPi pathway; L2: the same model as L1 with a further lesion of local collaterals in GPi.

Using this model, we set out to answer the following: is this the right mix of responses for therapeutically effective DBS in STN? Does a "mixture of response" perspective offer an explanation for why STN DBS is therapeutically effective at greater than 100 Hz (Deep Brain Stimulation for Parkinson's Disease Study Group, 2001)? And does it offer some clues to why an optogenetic model of STN DBS might not work (Gradinaru et al., 2009)?

Model replicates mix of rate and pattern responses during STN DBS in awake, MPTP primate

We first assessed whether our simulated STN DBS created the mix of responses in the basal ganglia output corresponding to therapeutically effective DBS in STN. To do so, we set out to replicate the data on neuron response changes from a study of STN DBS in the MPTP primate model (Hashimoto et al., 2003; Hahn et al., 2008). We chose this study as it is both the most complete data-set of changes in STN target nuclei under known therapeutic STN high-frequency stimulation and because there is a detailed analysis of individual neuron responses due to Hahn et al. (2008). Our work here complemented that of Hahn & McIntyre (2010), who searched over parameters of a computational model of the STN-GPe-GPi circuit to fit the mean firing and burst rates from recordings of the MPTP state off-DBS, and then showed how simulated STN DBS changed both these in accord with the experimental data. We extended this by showing how a pre-existing model of the basal ganglia can, by changing only the $I_{\max}$ parameter of our DBS model, both replicate the changes in mean rate and regularity and the mix of individual neuron responses.

We assessed the model's replication of STN stimulation-induced changes in both spike rate and regularity for different values of peak DBS current $I_{\max}$. For replication of changes in firing rate, we measured: (i) the percentage change in mean rate from pre-DBS to on-DBS epochs from recorded neurons in GPi and GPe, and (ii) the proportion of those recorded neurons that showed a significant increase, a significant decrease, and no change in firing rate. For replication of changes in spike regularity, we measured the percentage changes in ISI CV from pre-DBS to on-DBS epochs from recorded neurons in GPi. To compare to data, we first extracted individual neuron ISI CV responses from Figure 2 of Hahn et al. (2008): in the experimental recordings, the mean ISI CV in GPi did not significantly differ between pre-DBS and on-DBS epochs (Hahn et al., 2008); however, individual neurons had large changes in regularity, with a mean increase of 40.4±13.28% (n=12) and mean decrease of -27 ± 2.91% (n=24). So we assessed the replication of: (iii) the proportion of neurons that showed an increase and decrease of ISI CV; (iv) the mean percentage change in ISI CV for increasing neurons; (v) the mean percentage

change in ISI CV for decreasing neurons; and (vi) the ensemble mean ISI CV not significantly differing between pre-DBS and on-DBS (two-tailed t-test, at $p = 0.05$). Thus, in total we assessed six measures of fit between GPi output in model and data.

For both rate and regularity we assessed percentage changes because, as our model was explicitly of the rat basal ganglia, so its tonic rates in STN, GPe, and GPi were considerably less than those recorded in primate: thus we assessed magnitude changes, not exact values. To ensure comparable statistics and sampling of distributions between models and data we replicated the study design (see Materials and methods): the Hashimoto et al. (2003) study used 2 monkeys, and Hahn et al. (2008) analysed a total of 20 GPe neurons and 36 GPi neurons recorded from both in pre-DBS and on-DBS epochs. Thus for each simulation of the Hashimoto et al. (2003) study, we used 2 instantiations of the model, sampling 10 GPe cells and 18 GPi cells from each.

Figure 3 shows that the model replicated all tested firing rate changes in the basal ganglia output during STN high frequency stimulation: the percentage change in mean rate of GPi neurons and the sampled mix of responses (increase, decrease, no change) in GPi. These were simultaneously replicated across most tested values of $I_{\max}$. The firing rate responses of GPi in the MPTP primate were thus robustly well-fit. Figure 3 shows that, over a narrower range of $I_{\max}$ ($\sim 1000 - 1500$ pA), the model also simultaneously replicated the change in mean rate and sampled mix of responses in GPe.

Figure 4 shows that the model replicated all tested GPi spike-train regularity changes during STN high frequency stimulation: the mix of ISI CV responses (increase, decrease); the mean percentage change in ISI CV for neurons with increasing ISI CV; the mean percentage change for neurons with decreasing ISI CV; and the non-significant difference in mean ISI CV between pre-DBS and on-DBS epochs. Simultaneous replications of all regularity measures were robust across the lower range of $I_{\max}$ ($\sim 250 - 1500$ pA).

Across all fits to rate changes and mix of responses in GPi and GPe, and to ISI CV changes and mix of responses in GPi, the choice of $I_{\max} = 1500$ pA was best able to simultaneously replicate all these data properties (we quantify this statement in the next section). Thus we used this value for further DBS simulations when assessing therapeutic effects.

The mixture of responses is robust to model variations

These results showed that the DBS-evoked mixture of rate and regularity responses, generated solely by the network of our model, were consistent with the mixture of rate and regularity responses seen under therapeutic STN DBS

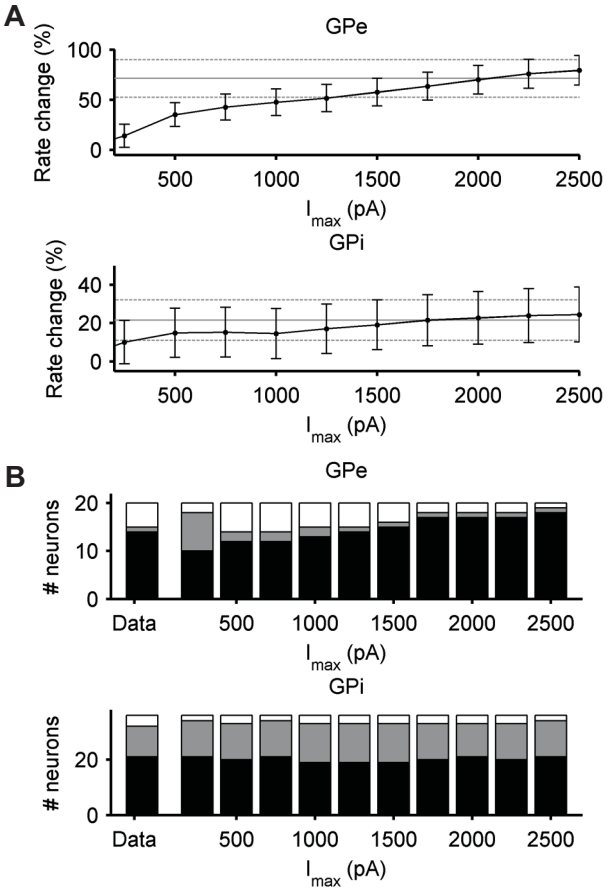

Figure 3: Model replicates magnitude and mixture of rate changes in a primate DBS study. (A) Percentage change in mean rate caused by high-frequency STN stimulation. Increasing the DBS current magnitude ($I_{\max}$) caused a larger increase in mean firing rates in both GPe and GPi. For $I_{\max} \gtrsim 1000$ pA, the model was able to reproduce closely the magnitude rate changes observed in both GPe and GPi of primate. Model plotted as mean $\pm$ s.e.m. Grey lines give the target data: mean (solid) ± 1 s.e.m. (dashed) percentage change in rates in response to STN DBS in MPTP primate model (Hashimoto et al., 2003; Hahn et al., 2008). (B) Mixture of responses in sampled neurons. Increasing $I_{\max}$ increased the number of excitatory responses (black) in GPe, correspondingly decreasing the occurrence of both inhibitory responses (grey), and no change (white). By contrast, the mix of responses in GPi was stable to the changes in $I_{\max}$. The mix of responses observed under STN DBS in the MPTP primate model (Hashimoto et al., 2003; Hahn et al., 2008) was closely reproduced in GPe over 500 to 1500 pA, and closely reproduced in GPi for all tested currents. Data are given in the left-most bars.

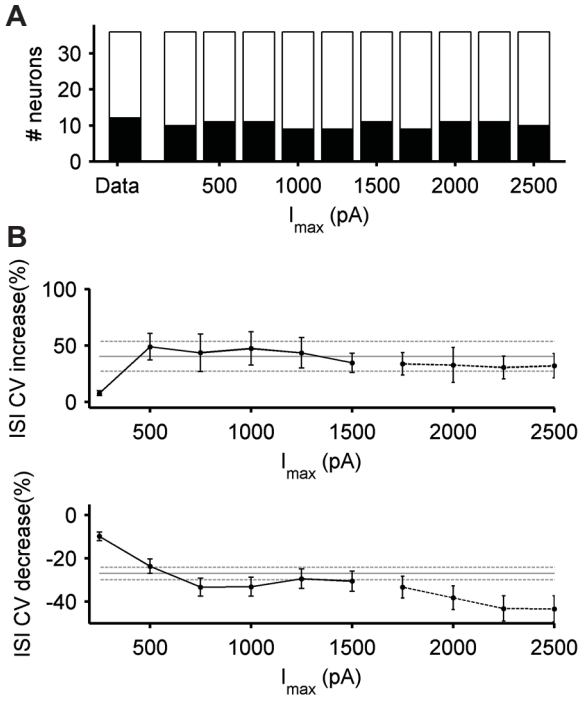

Figure 4: Model replicated the magnitude and mixture of changes in GPi spike-train regularity from a primate DBS study. Regularity was measured by the coefficient of variation (CV) of the inter-spike intervals (ISI). (A) The mixture of GPi neurons showing an increased (black) or decreased (white) ISI CV during STN high frequency stimulation. For all tested maximum current size $I_{\max}$, the ratio of CV response directions matched that of the data (Hashimoto et al., 2003; Hahn et al., 2008), given in the left-most bar. (B) Magnitude change in ISI CV caused by high-frequency STN stimulation. Top: mean percentage change for neurons with increased ISI CV; bottom: mean percentage change for neurons with decreased ISI CV. For $I_{\max} \leq 1500$pA, the model was able to closely reproduce the same magnitude changes observed for both increasing and decreasing ISI CV neurons; moreover it was able to reproduce the non-significant difference of the overall mean ISI CV between pre- and on-stimulation epochs (black dashed line indicates range of $I_{\max}$ that gave a significant difference in mean ISI CV between pre-DBS and on-DBS epochs). Model data plotted as mean $\pm$ s.e.m. Grey lines: mean (solid) $\pm$ s.e.m. (dashed) percentage change in ISI CV in response to STN DBS in MPTP primate model (Hashimoto et al., 2003; Hahn et al., 2008).

in primates. To further confirm the robustness of these results, we checked that plausible changes to the model still produced a mixture of responses in basal ganglia output, and replicated the primate data on STN DBS responses.

We checked three variants of the original model. The first variant omitted the discrete-channel architecture for the connections between basal ganglia structures. The presence of parallel loops running through the basal ganglia has strong support from anatomical studies (see e.g. Alexander & Crutcher, 1990; Hoover & Strick, 1993; Romanelli et al., 2005). Nonetheless, imposing discrete channels in our relatively small and densely connected model creates some correlation between the inputs to neurons in the same channel, which could plausibly affect the results. For the no-channel model variant, every neuron connected with probability $p = 0.25/3$ to any neuron in each of its target structures. In this way, the expected number of connections between structures were exactly equivalent between the channel-based and no-channel models.

The second variant omitted the local axon collaterals in GPi. As our model was originally of rat basal ganglia it explicitly modelled the SNr as the main basal ganglia output nucleus, and consequently included the well-described local axon collaterals in that structure (Deniau et al., 1982; Mailly et al., 2003). However, beyond a brief note of their existence (Parent et al., 2001), there has been little work establishing an equivalent network of local axon collaterals in primate GPi. We thus checked that their omission did not affect our results. Finally, the third variant shortened the NMDA synaptic current decay constant to 50 ms, the lowest plausible value in the basal ganglia (Gotz et al., 1997), to check that our results did not depend on prolonged excitation of GPe and GPi neurons by their STN inputs.

For each tested value of maximum DBS current I_{max}, we assessed each variant's error in reproducing the mixture of responses in GPi and in GPe (as in Figure 3B), and each variant's ability to fit *simultaneously* all other measures of rate and regularity changes between pre- and on-DBS epochs. We assessed fits to the same five measures as for the original model: the GPi and GPe mean rate (as in Figure 3A), mean GPi ISI CV increase and decrease (as in Figure 4B), and the non-significant difference between all GPi ISI CVs in the pre- and on-DBS epochs. For rate and ISI CV changes we used a conservative criterion for a fit to the data: that the mean values for model and data were within 1 s.e.m, as illustrated by the error bars for model and data plotted in Figures 3A and 4B.

Figure 5 shows that each model variant was able to reproduce the mixture of responses in GPi output evoked by STN DBS, with comparable error to the original model, while also still able to replicate all other tested measures of rate and regularity changes. Thus, the mixture of STN-DBS evoked responses in basal ganglia output resulting from the basal ganglia network is highly robust to plausible changes in the model. We noted that the original model was best able to reproduce the mixture of responses in GPe output while still fitting all other measures.

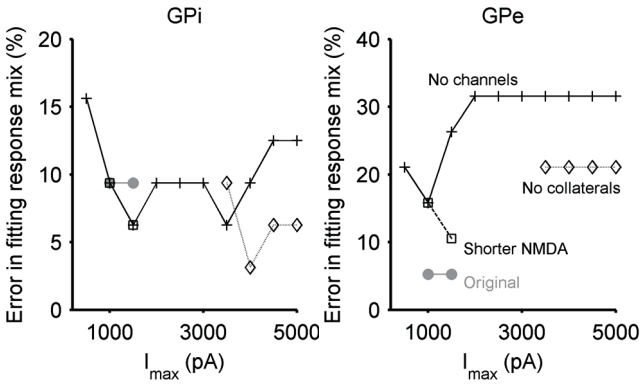

Figure 5: Robustness of model replication of STN DBS evoked responses in primate GPi and GPe (Hashimoto et al., 2003; Hahn et al., 2008). We plot the error for each model variant's fit to the mixture of responses in GPi (left) and GPe (right) observed under STN DBS in the MPTP primate model (data in the left-most bars of Figure 3B). Error is expressed as a percentage of the maximum error, which would be to assign all neurons to the smallest response category in the data. The plotted range of the lines shows the range of tested maximum DBS current I_{max} over which each model variant was also able to fit *simultaneously* all other measured GPi and GPe response properties in Figures 3 and 4. Under the conservative fitting criteria adopted here, the original basal ganglia model (grey circles) replicated all response properties between 1000 and 1500 pA. The model variants tested the effects of not imposing a discrete-channel architecture on the connections between structures (+), of omitting the local collaterals in GPi ($\diamond$), and of reducing the time constant for decay of NMDA-evoked post-synaptic currents ($\square$).

Consequently, we used this model for subsequent simulations.

Changing DBS frequency changes the mixture of rate and regularity responses

A key unknown in understanding how DBS works is why the therapeutic frequency for treatment of Parkinson's Disease motor symptoms and tremor is normally above 100 Hz (Limousin et al., 1995; Deep Brain Stimulation for Parkinson's Disease Study Group, 2001; Volkmann et al., 2002). Here we show, using parameters for the DBS model established above, our model predicts that basal ganglia output response patterns change dramatically with increasing DBS frequency, and a unique, stable balance of breadth of response and direction of response appears at therapeutic frequencies.

We assessed the model GPi neurons' firing rate and spike-train regularity changes in response to a range of STN stimulation frequencies. We found that the mixture of firing rate responses (increase, decrease, no change) in GPi became more stable above 100 Hz stimulation (Figure 6A), with a marked step-change in the proportion of inhibitory responses at 100 Hz stimulation (Figure 6A, right). Figure 6B shows that the distribution of percentage firing rate changes across the GPi became strongly skewed above 100 Hz stimulation. Moreover, the distributions

of changes were also stable for stimulation frequencies above 100 Hz (Figure 6B, right). Thus, in addition to GPi neurons becoming strongly excited and entrained by STN stimulation, the larger proportion of significantly inhibitory responses included GPi neurons that became silenced only by stimulation above 100 Hz.

We found that the mixture of ISI CV direction changes in GPi was not markedly altered by stimulation frequencies above 75 Hz (Figure 6C). However, Figure 6D shows that the distribution of ISI CV changes in GPi became strongly asymmetric above 100 Hz. Moreover, the distributions of changes were also stable for stimulation frequencies above 100 Hz (Figure 6D, right). Thus, while the proportion of GPi neurons showing increases and decreases in spike-train regularity did not markedly change at therapeutic stimulation frequencies, the magnitude of those changes did.

Optogenetic model DBS alters the response mix compared to electrical DBS model

Our results suggest that a specific mix of basal ganglia output rate and regularity changes is found under therapeutic STN DBS. We wondered if this observation could help explain why using an optogenetic model of STN excitation by DBS failed to find any therapeutic effect in parkinsonian rats (Gradinaru et al., 2009).

In an innovative use of recent developments in optogenetic technology, Gradinaru et al. (2009) addressed the controversy over the effect of high frequency stimulation on the STN by driving spiking activity in channel-rhodopsin expressing STN neurons with 130 Hz light pulses. However, they found that such unambiguous direct 130 Hz stimulation of STN neurons did not alleviate behavioural deficits in parkinsonian rats. These results present a stern challenge to the idea that elevated, regularised STN spiking activity – whether axonally or somatically induced – is key to the effectiveness of standard, electrical DBS.

We considered this difficulty from the perspective that a specific mix of responses in basal ganglia output is the main cause of STN DBS effectiveness. We noted that Gradinaru et al.'s (2009) excitation of STN was exceptionally uniform: they estimated almost all neurons ($95.73 \pm 1.96\%$) were infected with the channel-rhodopsin promoter CaMKII, and thus likely to express the light-sensitive ion channels; further, they estimated that the wavelength of light used was able to penetrate the whole volume of rodent STN (~ 0.7 mm^3) at a sufficient intensity to active the light-sensitive ion channels. We hypothesised that this uniform excitation was the key to the ineffectiveness of an optogenetic-DBS model.

To test this, we compared the output of our basal ganglia model under an optogenetic-DBS model to the electrical-DBS model established in the preceding sections. To mimic the uniform take up and light penetration,

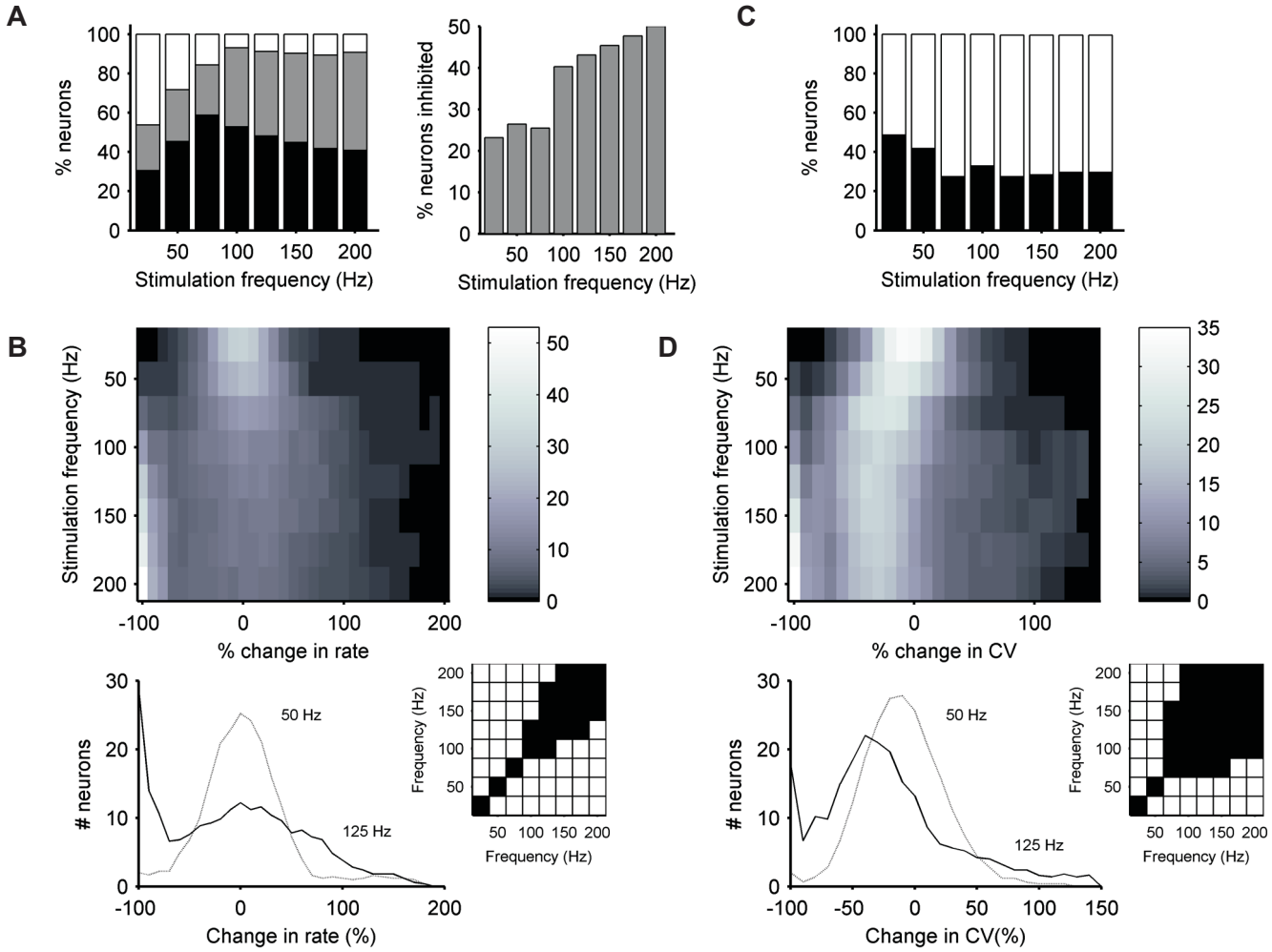

Figure 6: High-frequency stimulation of STN causes a unique pattern of changes in basal ganglia output. (A) Left: The mixture of GPi neurons showing an excitatory (black), inhibitory (grey), or no firing rate response at each stimulation frequency. Right: re-plotting the proportion of inhibitory responses at each stimulation frequency. (B) Top: The distribution of firing rate changes for each stimulation frequency. Colour intensity indicates number of neurons. Bottom: re-plotting the distributions at 50 and 125 Hz, illustrating the shift from symmetric to asymmetric distribution of firing rate changes above 100 Hz, including the jump in silenced neurons (-100 % change). Right: significant (white) and non-significant (black) differences between the distributions of firing rate changes at each DBS frequency (Kolmogrov-Smirnov test, at $p = 0.05$); the non-significant differences illustrate the stability of the distributions for stimulation frequencies above 100 Hz. (C) The mixture of GPi neurons showing an increased (black) or decreased (white) ISI CV at each stimulation frequency. (D) Top: The distribution of changes in ISI CV for each stimulation frequency. Colour intensity indicates number of neurons. Bottom: re-plotting the distributions at 50 and 125 Hz, illustrating the shift from symmetric to asymmetric distribution of changes in ISI CV above 100 Hz. Right: significant (white) and non-significant (black) differences between the distributions of ISI CV changes at each DBS frequency (Kolmogrov-Smirnov test, at $p = 0.05$); the non-significant differences illustrate the stability of the distributions for stimulation frequencies above 100 Hz.

we modelled optogenetic-like stimulation of STN by applying the same magnitude current pulse I_{DBS} to every STN neuron. We first estimated an appropriate magnitude of current pulse to mimic the optogenetic stimulation by fitting the change in STN firing rate during the optogenetic stimulation (Gradinaru et al., 2009).

Gradinaru et al. (2009) reported an $\sim 100\%$ increase in STN firing rate in response to 130 Hz light stimulation, recorded in 6-OHDA lesioned rats under isoflurane anaesthesia (whereas they tested the therapeutic effects of the optogenetic-DBS model in awake, freely-moving rodents). Thus we first found the appropriate magnitude of current pulse under isoflurane-like conditions, then applied it to awake, freely-moving rat like conditions. Isoflurane systemically increases the efficacy of GABAa synapses (Krasowski & Harrison, 1999; Yamakura & Harris, 2000), and causes global slow-wave activity at ~ 1 Hz in cortex (e.g. Ferron et al., 2009). As these physiological effects of isoflurane are very similar to urethane (Rudolph & Antkowiak, 2004), we adopted a similar approach to our previous simulations of urethane's effect on the basal ganglia (Humphries et al., 2006): cortical input oscillated at 1 Hz with an average firing rate of 24 spikes/s (see Materials and methods), and we increased GABAa synaptic weights by a factor of 1.5. Under this isoflurane-condition model, we tried a range of I_{DBS} uniformly applied at 130 Hz to every STN neuron during the on-DBS epoch. Following Gradinaru et al. (2009), for each tested I_{DBS} we computing the mean firing rate over 5 sampled STN neurons for the pre-DBS and on-DBS epochs. Figure 7A shows that $I_{\mathrm{DBS}} = 45$ pA was able to accurately reproduce the reported increase in STN firing rate during optogenetic-DBS.

We then compared the basal ganglia output responses for the optogenetic DBS model (with $I_{\mathrm{DBS}} = 45$ pA) to our electrical DBS model (Equation 2, using the best-fit to the Hashimoto et al. (2003) data of $I_{\max} = 1500$ pA, resulting in the distribution of I_{DBS} in Figure 1C). We ran ten models of awake, freely-moving, 6-OHDA rodent basal ganglia (Gradinaru et al., 2009), with each model run twice: once with the optogenetic-DBS model and once with the electrical-DBS model applied during the on-DBS epoch.

Figure 7B shows that the two DBS protocols differed markedly in their distribution of STN neuron fidelity to the DBS frequency: skewed towards high fidelity for the optogenetic-DBS stimulation model; bimodal in the electrical DBS model. We noted that this distribution of fidelity in the optogenetic-DBS model is in keeping with the known fidelity of channel-rhodopsin expressing neurons to regular, high frequency, pulsed light stimulation (Arenkiel et al., 2007).

Our models showed that, with these differing STN response distributions, the optogenetic-DBS and electrical-DBS models had multiple differences in the mix of responses in the basal ganglia output. First, optogenetic-DBS caused many more excitatory responses in GPi than electrical-DBS (Figure 7C). Second, optogenetic-DBS

generally caused higher fidelity of GPi firing to the STN stimulation frequency, particularly in the regime of near 1:1 fidelity, than electrical-DBS (Figure 7D). Third, optogenetic-DBS increased the regularity of GPi neuron firing more than electrical-DBS (Figure 7E). Consequently, with the increased fidelity and increased regularity of firing, optogenetic-DBS caused more tightly-correlated firing between GPi neuron pairs than electrical-DBS (Figure 7F). Thus our models show that optogenetic-like DBS and electrical-like DBS differ in their effects on rate, regularity and correlation of the basal ganglia output.

Discussion

We set out to begin addressing the hypothesis that a mixture of responses in the basal ganglia output nuclei, combining regularised firing and inhibition, is a key contributor to the effectiveness of STN DBS. Here we had two goals: first, to use our computational model of the complete basal ganglia circuit (Humphries et al., 2006) to understand how such a mixture of responses in basal ganglia output may arise from the network effects of STN DBS; second, we sought whether, from this "mixture of responses" perspective, the model could suggest resolutions to two DBS puzzles: the therapeutically effective range of frequencies, and the ineffectiveness of direct-activation optogenetic models of STN DBS. We showed that the model predicts a mixture of responses in the basal ganglia output arising as a natural consequence of the network effects of STN DBS. We replicated the diversification of responses recorded in a primate STN DBS study (Hashimoto et al., 2003; Hahn et al., 2008) to show that the model's predicted mixture of responses is consistent with therapeutic STN DBS. We then showed how, from this "mixture of response" perspective, the model suggested the respective hypotheses for the two puzzles: that the mixture of responses in basal ganglia output undergoes a step-change at therapeutic DBS frequencies; and that optogenetic-DBS models failed because their uniform stimulation of STN did not produce the putative therapeutically-effective mixture of responses evoked by standard, electrical DBS.

STN DBS drives a mixture of responses in basal ganglia output

We have shown that STN DBS can induce a mix of excitatory and inhibitory responses in the basal ganglia output nuclei, with some neurons entrained to stimulation frequency and others strongly inhibited. This mix of responses arose purely from the basal ganglia network: simulated STN DBS only affected STN neurons, and we did not simulate other hypotheses for the distal action of DBS, including recruitment of passing axon fibres or antidromic activation of STN afferents (McIntyre et al., 2004; McIntyre & Hahn, 2010; Bosch et al., 2011). Nonetheless, this

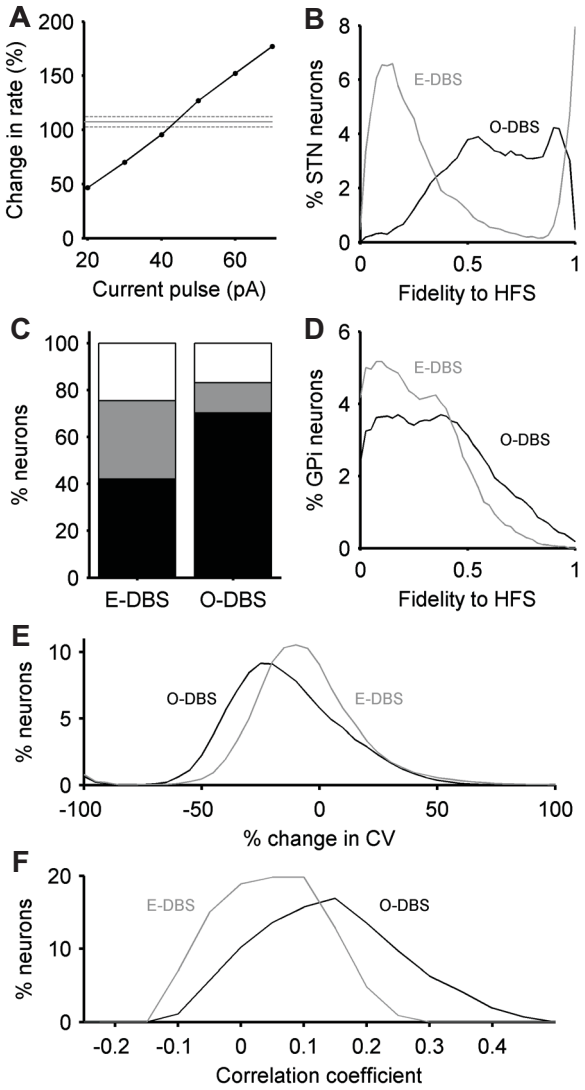

Figure 7: Simulated STN optogenetic-DBS and electrical-DBS create different mixtures of responses in basal ganglia output. (A) Tuning the optogenetic-DBS model. Mean increase in STN rate for a range of I_{DBS}, under simulated isoflurane-anaesthetised rat conditions. Grey lines give mean ± 2 s.e.m increase of STN firing during optogenetic-DBS stimulation in the same conditions recorded by Gradinaru et al. (2009). (B) Fidelity of STN neuron firing to 130 Hz stimulation in the optogenetic-DBS (O-DBS) and electrical-DBS (E-DBS) models. (All data here and in subsequent panels taken from DBS applied in models of awake, freely-moving rat). (C) The mixture of GPi neurons showing an excitatory (black), inhibitory (grey), or no (white) firing rate response to 130 Hz stimulation by optogenetic and electrical DBS models (mean over ten models). (D) Fidelity of GPi neuron firing to the 130 Hz simulation of STN in the optogenetic-DBS (O-DBS) and electrical-DBS (E-DBS) models. (E) The distribution of ISI CV changes in GPi caused by each type of DBS model (mean over ten models). (F) The distribution of spike correlations between neuron pairs caused by each type of DBS model. Correlation coefficients were computed between 200 randomly chosen pairs from the tenth model; their spike-trains during the on-DBS epoch were binned at 2.5 ms.

mix of responses in both spike rate and regularity accurately reflected those observed following therapeutic STN DBS in parkinsonian primates (Hashimoto et al., 2003; Hahn et al., 2008). Our model replicated the mixture of GPe and GPi neurons' firing rate responses and the mean percentage changes in GPe and GPi firing rate following STN high frequency stimulation; it also replicated the mixture of GPi neurons' changes in spike-train regularity, the respective mean percentage increase and decrease, and the non-significant change in overall mean regularity following STN high frequency stimulation. The model thus showed how the DBS results in this study were consistent with a purely network effect of STN DBS. We also showed that replication of these results was not dependent on a number of modelling assumptions (the imposition of a discrete-channel architecture, the presence of collaterals in GPi, nor the precise time-course of NMDA synaptic currents). Our results thus support the idea that a main contributor to the therapeutic effectiveness of STN DBS is its network effect, which creates a mixture of responses in the basal ganglia output through the balance of STN-originating excitation and GPe-originating inhibition arriving at the GPi (Kita et al., 2005; McIntyre & Hahn, 2010; Bosch et al., 2011; Reese et al., 2011).

STN DBS frequency determines the mixture of responses

The therapeutically-effective frequency of STN DBS is typically above 100 Hz in human patients (Deep Brain Stimulation for Parkinson's Disease Study Group, 2001). While stimulation frequencies in this range may enable STN neuron firing to track the DBS pulses (Garcia et al., 2005), our model suggests a network-based explanation for this range. We found that increasing stimulation frequency to the effective range for DBS caused a step change in the basal ganglia output's response characteristics. The distributions of both spike rate and spike regularity changes became strongly skewed above 100 Hz, reflecting the appearance of GPi neurons that were strongly entrained or silenced by STN DBS; moreover, the proportion of inhibitory responses in GPi non-linearly increased at 100 Hz. The model's results are thus consistent with a transition from symmetric to asymmetric effects of STN DBS on basal ganglia output at therapeutic frequencies.

Optogenetic-DBS may alter the mixture of responses

Gradinaru et al. (2009) recently used optogenetics to address the controversy over the effect of DBS on the STN. They tested the hypothesis that DBS directly activates STN neurons, by driving spiking activity in channelrhodopsin expressing STN neurons with 130 Hz light pulses. However, they found that such direct 130 Hz stimulation of STN neurons did not alleviate behavioural deficits in parkinsonian rat models, strongly challenging the

idea that elevated and regularised STN spiking activity alone underpins the effectiveness of standard, electrical DBS. To address this, we simulated optogenetic-DBS as a uniform stimulation of STN neurons, with a stimulating current pulse tuned to fit the reported change in STN firing rate following the onset of optogenetic-DBS (Gradinaru et al., 2009). The model showed that optogenetic-DBS stimulation was unable to provide the same diversity of responses in basal ganglia output as the electrical DBS stimulation: optogenetic-DBS predominantly caused an increased firing rate in GPi output, and a corresponding increase in regular, stimulation-tracking, firing and in the correlation of GPi neuron output. If the effectiveness of STN DBS indeed rests on a particular mixture of responses, then this may explain why a direct-excitation optogenetic model of STN DBS, causing uniform stimulation of STN neurons, did not result in the effective alleviation of motor symptoms in the parkinsonian rat (Gradinaru et al., 2009). Thus, in addition to other possible contributors to the therapeutic failure of the optogenetic model of STN DBS (such as millisecond different time-scales of STN neuron synchronisation by electrical and light stimulation), our model offers a novel network-based hypothesis.

Why then, from this perspective, did Gradinaru et al. (2009) find that optogenetic high frequency stimulation of either all layer 5 cortical terminals in STN or layer 5 neurons in motor cortex could alleviate the parkinsonian motor symptoms? As they noted, these results are consistent with the therapeutic effect of electrical STN DBS arising from antidromic activation of these cortical neurons. We note though that both stimulations could cause a non-uniform excitation of STN neurons. In both cases, whether stimulating all cortical afferents from layer 5 or just those with somas in the motor cortex layer 5, these make up only a subset of glutamatergic projections to STN neurons. A major glutamatergic input arises from parafasicular thalamus (Bevan et al., 1995), and others from across the upper brainstem (Bevan & Bolam, 1995). Thus, the stimulated terminals or neurons will be differentially distributed across the STN, with some STN neurons strongly innervated by layer 5 cortical neurons and others more weakly innervated. Moreover, as the optogenetic stimulation in both cases was driving synaptic input to the STN and not direct spiking, it is likely more susceptible to modulation by GABAergic input from GPe. Thus, we speculate that optogenetic high frequency stimulation of layer 5 terminals or somas has a similar effect on STN neurons to the spreading current model of electrical DBS used here, thus resulting in the mixture of basal ganglia output responses corresponding to therapeutic DBS.

How might a mixture of responses to DBS restore function?

We have used computational models here to generate mechanistic hypotheses for the action of STN high frequency stimulation on basal ganglia output nuclei, and for the effectiveness of DBS. The next, crucial step will be to address if and why such a mix of responses is key to the restorative effect of DBS. We comment on three perspectives here. First, from the perspective that DBS restores function to the targets of the basal ganglia by output regularisation. Elegant studies by Rubin and colleagues (Rubin & Terman, 2004; Guo et al., 2008) and by Dorval et al. (2010) have provided compelling demonstrations of how, by regularising basal ganglia output to thalamus, STN DBS may improve thalamo-cortical neurons' transmission of their excitatory inputs. Our results are consistent with STN DBS regularising the output of a subset of GPi neurons, and hence the reinstatement of thalamic information transfer; but our results also point to the silencing of a substantial number, and a mixture of responses in the rest of basal ganglia output. The studies of thalamo-cortical relay fidelity have typically considered the effect of one or a few GPi inputs, on an isolated thalamo-cortical cell, relaying one type of input (a pulsed current), and using one model of error in thalamic information transfer (a 1:1 spike-locking regime). Consequently, in the context of full basal ganglia-thalamo-cortical circuit or of other models of thalamic information transfer to cortex (such as the necessary synchronisation of thalamo-cortical neurons, Bruno & Sakmann, 2006; Bruno, 2011), it may turn out that regularising all basal ganglia output simply overwrites one form of pathological activity with another, artificially generated form. Indeed, a prediction of our model is that the optogenetic-DBS model failed to alleviate parkinsonian motor symptoms (Gradinaru et al., 2009) because it over-regularised the basal ganglia output. Thus, one possibility is that a balance of regularisation and inhibition amongst the basal ganglia output neurons is necessary for the restoration of thalamic relay fidelity.

Second, we consider how DBS might restore function to targets of the basal ganglia output through the seemingly paradoxical removal of inhibition. The dominant theory of basal ganglia function is that they operate by disinhibition – signalling the selection of motor programs by selectively reducing their tonic inhibitory output to their target structures (Mink, 1996; Redgrave et al., 1999; Hikosaka et al., 2000). The therapeutic success of STN DBS, and its activation of basal ganglia output nuclei (Hashimoto et al., 2003; Shi et al., 2006; Bosch et al., 2011; Moran et al., 2011; Reese et al., 2011), is a considerable challenge to this theory (Nambu, 2008): for how can stimulating the STN alleviate motor symptoms, when it increases the activity of basal ganglia output, and consequently increases, not reduces, their tonic inhibition of target structures? Our results suggest a resolution: that, through its network effect, STN DBS actually generates widespread, permanent inhibition of much basal ganglia

output, including the silencing of a number of neurons (see Figure 6A, right). Consequently, STN DBS would reduce permanently the tonic inhibition of a subset of neurons in the basal ganglia target structures, allowing them to respond to their other inputs. Moreover, we showed that this inhibition of basal ganglia output was consistent with the effects of therapeutically-effective STN DBS on primate GPi (Hashimoto et al., 2003; Hahn et al., 2008). Thus our model shows how both information transfer through and disinhibition of basal ganglia target nuclei could be reinstated by STN DBS.

Finally, a view-point strangely lacking from theoretical STN DBS studies to date, is how it might re-enable information flow through the basal ganglia from the striatum to its outputs (Hammond et al., 2007). That is, in both the above perspectives, STN DBS restores function to target structures through permanently altering basal ganglia output, but they do not address if or how STN DBS restores function to the basal ganglia through re-instating control over that output. Our results suggest a preliminary observation. In our model, the mixture of responses to STN DBS amongst the basal ganglia output neurons is underpinned by each neuron's balance of excitatory input from STN and GABAergic input from GPe and local collaterals. By reinstating the dominance of inhibition over some basal ganglia output neurons and the dominance of excitation over others, STN DBS may thus allow phasic inhibitory input from striatum to again modulate basal ganglia outflow, and reinstate basal ganglia computation (Mink, 1996; Redgrave et al., 1999; Gurney et al., 2001; Humphries et al., 2006; Leblois et al., 2006a). Understanding if such a mixture of responses is indeed key to restoration of function in the basal ganglia is our next challenge.

References

Alexander, G. E. & Crutcher, M. D. (1990). Functional architecture of basal ganglia circuits: neural substrates of parallel processing. *Trends in Neuroscience*, **13**, 266–272.

Arenkiel, B. R., Peca, J., Davison, I. G., Feliciano, C., Deisseroth, K., Augustine, G. J., Ehlers, M. D., & Feng, G. (2007). In vivo light-induced activation of neural circuitry in transgenic mice expressing channelrhodopsin-2. *Neuron*, **54**, 205–218.

Beurrier, C., Bioulac, B., Audin, J., & Hammond, C. (2001). High-frequency stimulation produces a transient blockade of voltage-gated currents in subthalamic neurons. *J Neurophysiol*, **85**, 1351–1356.

Beurrier, C., Congar, P., Bioulac, M., & Hammond, C. (1999). Subthalamic nucleus neurons switch from single spike-activity to burst-firing mode. *J Neurosci*, **19**, 599–609.

Bevan, M. D. & Bolam, J. P. (1995). Cholinergic, GABAergic, and glutamate-enriched inputs from the mesopontine tegmentum to the subthalamic nucleus in the rat. *J Neurosci*, **15**, 7105–7120.

Bevan, M. D., Francis, C. M., & Bolam, J. P. (1995). The glutamate-enriched cortical and thalamic input to neurons in the subthalamic nucleus of the rat: Convergence with GABA-positive terminals. *J Comp Neurol*, **361**, 491–511.

Bevan, M. D., Magill, P. J., Hallworth, N. E., Bolam, J. P., & Wilson, C. J. (2002). Regulation of the timing and pattern of action potential generation in rat subthalamic neurons in vitro by GABA-A IPSPs. *J Neurophysiol*, **87**, 1348–1362.

Birdno, M. J., Cooper, S. E., Rezai, A. R., & Grill, W. M. (2007). Pulse-to-pulse changes in the frequency of deep brain stimulation affect tremor and modeled neuronal activity. *J Neurophysiol*, **98**, 1675–1684.

Birdno, M. J. & Grill, W. M. (2008). Mechanisms of deep brain stimulation in movement disorders as revealed by changes in stimulus frequency. *Neurotherapeutics*, **5**, 14–25.

Bosch, C., Degos, B., Deniau, J.-M., & Venance, L. (2011). Subthalamic nucleus high-frequency stimulation generates a concomitant synaptic excitation-inhibition in substantia nigra pars reticulata. *J Physiol*, **589**, 4189–4207.

Bruno, R. M. (2011). Synchrony in sensation. *Curr Opin Neurobiol*, **21**, 701–708.

Bruno, R. M. & Sakmann, B. (2006). Cortex is driven by weak but synchronously active thalamocortical synapses. *Science*, **312**, 1622–1627.

Deep Brain Stimulation for Parkinson's Disease Study Group (2001). Deep-brain stimulation of the subthalamic nucleus or the pars interna of the globus pallidus in Parkinson's disease. *N Engl J Med*, **345**, 956–963.

Deniau, J. M., Kitai, S. T., Donoghue, J. P., & Grofova, I. (1982). Neuronal interactions in the substantia nigra pars reticulata through axon collaterals of the projection neurons. an electrophysiological and morphological study. *Exp Brain Res*, **47**, 105–113.

Dorval, A. D., Kuncel, A. M., Birdno, M. J., Turner, D. A., & Grill, W. M. (2010). Deep brain stimulation alleviates parkinsonian bradykinesia by regularizing pallidal activity. *J Neurophysiol*, **104**, 911–921.

Ferron, J.-F., Kroeger, D., Chever, O., & Amzica, F. (2009). Cortical inhibition during burst suppression induced with isoflurane anesthesia. *J Neurosci*, **29**, 9850–9860.

Garcia, L., Audin, J., D'Alessandro, G., Bioulac, B., & Hammond, C. (2003). Dual effect of high-frequency stimulation on subthalamic neuron activity. *J Neurosci*, **23**, 8743–8751.

Garcia, L., D'Alessandro, G., Fernagut, P.-O., Bioulac, B., & Hammond, C. (2005). Impact of high-frequency stimulation parameters on the pattern of discharge of subthalamic neurons. *J Neurophysiol*, **94**, 3662–3669.

Gotz, T., Kraushaar, U., Geiger, J., Lubke, J., Berger, T., & Jonas, P. (1997). Functional properties of AMPA and NMDA receptors expressed in identified types of basal ganglia neurons. *J Neurosci*, **17**, 204–215.

Gradinaru, V., Mogri, M., Thompson, K. R., Henderson, J. M., & Deisseroth, K. (2009). Optical deconstruction of parkinsonian neural circuitry. *Science*, **324**, 354–359.

Guo, Y., Rubin, J. E., McIntyre, C. C., Vitek, J. L., & Terman, D. (2008). Thalamocortical relay fidelity varies across subthalamic nucleus deep brain stimulation protocols in a data-driven computational model. *J Neurophysiol*, **99**, 1477–1492.

Gurney, K., Prescott, T. J., & Redgrave, P. (2001). A computational model of action selection in the basal ganglia I: A new functional anatomy. *Biol Cybern*, **85**, 401–410.

Hahn, P. J. & McIntyre, C. C. (2010). Modeling shifts in the rate and pattern of subthalamopallidal network activity during deep brain stimulation. *J Comput Neurosci*, **28**, 425–441.

Hahn, P. J., Russo, G. S., Hashimoto, T., Miocinovic, S., Xu, W., McIntyre, C. C., & Vitek, J. L. (2008). Pallidal burst activity during therapeutic deep brain stimulation. *Exp Neurol*, **211**, 243–251.

Hammond, C., Bergman, H., & Brown, P. (2007). Pathological synchronization in Parkinson's disease: networks, models and treatments. *Trends Neurosci*, **30**, 357–364.

Hashimoto, T., Elder, C. M., Okun, M. S., Patrick, S. K., & Vitek, J. L. (2003). Stimulation of the subthalamic nucleus changes the firing pattern of pallidal neurons. *J Neurosci*, **23**, 1916–1923.

Hikosaka, O., Takikawa, Y., & Kawagoe, R. (2000). Role of the basal ganglia in the control of purposive saccadic eye movements. *Physiol Rev*, **80**, 953–978.

Hoover, J. E. & Strick, P. L. (1993). Multiple output channels in the basal ganglia. *Science*, **259**, 819–821.

Humphries, M. D. & Gurney, K. (2007a). Deep brain stimulation of the subthalamic nucleus causes paradoxical inhibition of output in a computational model of the "parkinsonian" basal ganglia. In *2007 Neuroscience Meeting Planner* pp. Program No. 622.9 San Diego, CA: Society for Neuroscience.

Humphries, M. D. & Gurney, K. (2007b). A means to an end: validating models by fitting experimental data. *Neurocomputing*, **70**, 1892–1896.

Humphries, M. D. & Gurney, K. N. (2001). A pulsed neural network model of bursting in the basal ganglia. *Neural Networks*, **14**, 845–863.

Humphries, M. D., Stewart, R. D., & Gurney, K. N. (2006). A physiologically plausible model of action selection and oscillatory activity in the basal ganglia. *J Neurosci*, **26**, 12921–12942.

Kita, H., Tachibana, Y., Nambu, A., & Chiken, S. (2005). Balance of monosynaptic excitatory and disynaptic inhibitory responses of the globus pallidus induced after stimulation of the subthalamic nucleus in the monkey. *J Neurosci*, **25**, 8611–8619.

Krasowski, M. D. & Harrison, N. L. (1999). General anaesthetic actions on ligand-gated ion channels. *Cell Mol Life Sci*, **55**, 1278–1303.

Leblois, A., Boraud, T., Meissner, W., Bergman, H., & Hansel, D. (2006a). Competition between feedback loops underlies normal and pathological dynamics in the basal ganglia. *J Neurosci*, **26**, 3567–3583.

Leblois, A., Meissner, W., Bezard, E., Bioulac, B., Gross, C. E., & Boraud, T. (2006b). Temporal and spatial alterations in GPi neuronal encoding might contribute to slow down movement in Parkinsonian monkeys. *Eur J Neurosci*, **24**, 1201–1208.

Limousin, P., Pollak, P., Benazzouz, A., Hoffmann, D., Bas, J. F. L., Broussolle, E., Perret, J. E., & Benabid, A. L. (1995). Effect of parkinsonian signs and symptoms of bilateral subthalamic nucleus stimulation. *Lancet*, **345**, 91–95.

Magill, P. J., Bolam, J. P., & Bevan, M. D. (2001). Dopamine regulates the impact of the cerebral cortex on the subthalamic nucleus-globus pallidus network. *Neuroscience*, **106**, 313–330.

Mailly, P., Charpier, S., Menetrey, A., & Deniau, J. M. (2003). Three-dimensional organization of the recurrent axon collateral network of the substantia nigra pars reticulata neurons in the rat. *J Neurosci*, **23**, 5247–5257.

McIntyre, C. C., Grill, W. M., Sherman, D. L., & Thakor, N. V. (2004). Cellular effects of deep brain stimulation: model-based analysis of activation and inhibition. *J Neurophysiol*, **91**, 1457–1469.

McIntyre, C. C. & Hahn, P. J. (2010). Network perspectives on the mechanisms of deep brain stimulation. *Neurobiol Dis*, **38**, 329–337.

Mink, J. W. (1996). The basal ganglia: Focused selection and inhibition of competing motor programs. *Prog Neurobiol*, **50**, 381–425.

Miocinovic, S., Parent, M., Butson, C. R., Hahn, P. J., Russo, G. S., Vitek, J. L., & McIntyre, C. C. (2006). Computational analysis of subthalamic nucleus and lenticular fasciculus activation during therapeutic deep brain stimulation. *J Neurophysiol*, **96**, 1569–1580.

Moran, A., Stein, E., Tischler, H., Belelovsky, K., & Bar-Gad, I. (2011). Dynamic stereotypic responses of basal ganglia neurons to subthalamic nucleus high-frequency stimulation in the parkinsonian primate. *Front Syst Neurosci*, **5**, 21.

Nambu, A. (2008). Seven problems on the basal ganglia. *Curr Opin Neurobiol*, **18**, 595–604.

Nisenbaum, E. S. & Wilson, C. J. (1995). Potassium currents responsible for inward and outward rectification in rat neostriatal spiny projection neurons. *J Neurosci*, **15**, 4449–4463.

Nowak, L. G. & Bullier, J. (1998). Axons, but not cell bodies, are activated by electrical stimulation in cortical gray matter. I. Evidence from chronaxie measurements. *Exp Brain Res*, **118**, 477–488.

Parent, M., Levesque, M., & Parent, A. (2001). Two types of projection neurons in the internal pallidum of primates: single-axon tracing and three-dimensional reconstruction. *J Comp Neurol*, **439**, 162–175.

Perlmutter, J. S. & Mink, J. W. (2006). Deep brain stimulation. *Annu Rev Neurosci*, **29**, 229–257.

Plenz, D. & Kitai, S. T. (1999). A basal ganglia pacemaker formed by the subthalamic nucleus and external globus pallidus. *Nature*, **400**, 677–682.

Ranck, J. B. (1975). Which elements are excited in electrical stimulation of mammalian central nervous system: a review. *Brain Res*, **98**, 417–440.

Rattay, F. (1999). The basic mechanism for the electrical stimulation of the nervous system. *Neuroscience*, **89**, 335–346.

Redgrave, P., Prescott, T. J., & Gurney, K. (1999). The basal ganglia: A vertebrate solution to the selection problem? *Neuroscience*, **89**, 1009–1023.

Reese, R., Leblois, A., Steigerwald, F., Ptter-Nerger, M., Herzog, J., Mehdorn, H. M., Deuschl, G., Meissner, W. G., & Volkmann, J. (2011). Subthalamic deep brain stimulation increases pallidal firing rate and regularity. *Exp Neurol*, **229**, 517–521.

Romanelli, P., Esposito, V., Schaal, D. W., & Heit, G. (2005). Somatotopy in the basal ganglia: experimental and clinical evidence for segregated sensorimotor channels. *Brain Res Brain Res Rev*, **48**, 112–128.

Rubin, J. E. & Terman, D. (2004). High frequency stimulation of the subthalamic nucleus eliminates pathological thalamic rhythmicity in a computational model. *J Comput Neurosci*, **16**, 211–235.

Rudolph, U. & Antkowiak, B. (2004). Molecular and neuronal substrates for general anaesthetics. *Nat Rev Neurosci*, **5**, 709–720.

Shi, L.-H., Luo, F., Woodward, D. J., & Chang, J.-Y. (2006). Basal ganglia neural responses during behaviorally effective deep brain stimulation of the subthalamic nucleus in rats performing a treadmill locomotion test. *Synapse*, **59**, 445–457.

Surmeier, D. J., Mercer, J. N., & Chan, C. S. (2005). Autonomous pacemakers in the basal ganglia: who needs excitatory synapses anyway? *Curr Opin Neurobiol*, **15**, 312–318.

Tai, C.-H., Boraud, T., Bezard, E., Bioulac, B., Gross, C., & Benazzouz, A. (2003). Electrophysiological and metabolic evidence that high-frequency stimulation of the subthalamic nucleus bridles neuronal activity in the subthalamic nucleus and the substantia nigra reticulata. *FASEB J*, **17**, 1820–1830.

Volkmann, J., Herzog, J., Kopper, F., & Deuschl, G. (2002). Introduction to the programming of deep brain stimulators. *Mov Disord*, **17 Suppl 3**, S181–S187.

Windels, F., Bruet, N., Poupard, A., Urbain, N., Chouvet, G., Feuerstein, C., & Savasta, M. (2000). Effects of high frequency stimulation of subthalamic nucleus on extracellular glutamate and GABA in substantia nigra and globus pallidus in the normal rat. *Eur J Neurosci*, **12**, 4141–4146.

Yamakura, T. & Harris, R. A. (2000). Effects of gaseous anesthetics nitrous oxide and xenon on ligand-gated ion channels. comparison with isoflurane and ethanol. *Anesthesiology*, **93**, 1095–1101.

Zhang, T. C. & Grill, W. M. (2010). Modeling deep brain stimulation: point source approximation versus realistic representation of the electrode. *J Neural Eng*, **7**, 066009.

Acknowledgements

This work was supported by the ANR NEUROBOT project and the EU Framework 7 IMCLEVER project. Parts of this work previously appeared in abstract form (Humphries & Gurney, 2007a).

Abbreviations

CV: coefficient of variation; DBS: deep brain stimulation; GPe: globus pallidus pars externa; GPi: globus pallidus pars interna; ISI: inter-spike interval; STN: subthalamic nucleus